Journal of Engineering Mathematics (2005) 52: 293–305
DOI 10.1007/s10665-004-1768-3

Incompressible granular flow from wedge-shaped hoppers

GRAHAM J. WEIR
Applied Mathematics, Industrial Research, P.O. B. 31-310, Lower Hutt, New Zealand
E-mail: g.weir@irl.cri.nz

Received 26 March 2003; accepted in revised form 30 July 2004

Abstract. The incompressible plastic flow equations for a Drucker-Prager yield law and a J_2 flow rule are shown not to allow a steady single radial velocity component, for flows from a wedge-shaped hopper. The corresponding equations for two components of velocity are considered, using a series expansion of Kaza and Jackson, which connects asymptotically to Jenike's radial solution. This asymptotic solution gives a poor model of mass flows about the orifice, and an improvement is obtained by considering the pressure variation along the axis of the wedge, but using the angular variations determined by the power-series method. Numerical difficulties occurred for certain parameter values, when solving the two-point boundary-value problem resulting from the asymptotic series method. The region of this parametric sensitivity is associated with an internal maximum in the pressure field, whose appearance tends to offer a conservative estimate for the mass-funnel flow transition.

Key words: granular flow, hopper, mass-funnel flow transition, mathematical model, radial flow

1. Introduction

Previous results from applying plasticity theory to granular flows from hoppers have led to apparently contradictory conclusions. Stability analyses [1,2] suggest the plastic flow equations are inherently ill-posed, which implies that the corresponding granular flows should be transient (since infinitesimal disturbances will grow exponentially rapidly) and the flow fields will contain shear banding, which are regions of high shear.

Experimental observations confirm that granular flows are both transient [3] and contain shear bands [4]. In apparent contradiction to these conclusions are the experimental observations that effectively steady predictable discharges of granular material occur from a large class of hoppers [5–7] and that the properties of these flows are approximately predicted by steady analyses of the plastic-flow equations.

Brennen and Pearce [8] analysed the discharge of an incompressible plastic material from a wedge-shaped hopper, and found promising agreement with their experimental observations of granular flows. The corresponding results for a conical hopper were derived by Nguyen *et al.* [9], again supporting the conclusion that the steady plastic-flow equations provide good agreement with the corresponding granular flows. This does not seem to be compatible with the predictions of stability analyses that granular flows should be inherently pathological.

A major difficulty with the plastic-flow equations is that no one has found an exact solution corresponding to discharge from a hopper. Jenike [10] has obtained an exact 'radial' solution, but as this solution ignores the inertial terms and does not allow for a region of zero pressure, its relationship to hopper flows about the orifice is obscure. The other analyses have all been approximate. Essentially all analyses have assumed or expanded about a single component of velocity. The initial aim of this paper is to ask if such one-component radial flows exist in steady plastic flows from a hopper.

After answering this question in the negative, the asymptotic series expansion of Kaza and Jackson [11] is used, which joins smoothly to the Jenike radial solution far above the orifice. The first term in this series expansion corresponds to the Jenike solution. This series expansion is then truncated at the second term, the resulting post-Jenike terms obtained, and the corresponding modification of the Jenike radial solution discussed, with special interest in the mass-flow–funnel-flow transition.

2. Mathematical analysis

This section assumes that a steady radial plastic flow is occurring in a wedge-shaped hopper, and satisfies a J_2 flow rule and the Drucker-Prager yield law. It is convenient to non-dimensionalise the dimensional pressure components p, the dimensional radius R and dimensional velocity U_1 through

$$p = \rho g R_1 P, \qquad R = R_1 r, \qquad U_1 = \sqrt{gR_1} u_1, \tag{1, 2, 3}$$

where R_1 is the radial position of the orifice, ρ is density, and g is gravitation acceleration. Subscripts of one are used to emphasise the one-dimensional nature of this section.

The variables P, r, and u_1 are now non-dimensional. Since we are assuming only a radial velocity component, and incompressible flow,

$$u_1 = -\frac{T(\theta)}{r}, \tag{4}$$

where T is a function of only θ, the cylindrical angle, and the minus sign has been chosen because the flow direction out of the hopper is opposite to the radial direction.

The non-dimensional Newton-force equations for this steady radial flow are

$$u_1 u_{1,r} + P_{11,r} + \frac{1}{r} P_{12,\theta} + \frac{(P_{11} - P_{22})}{r} = -\cos\theta, \tag{5}$$

$$P_{12,r} + \frac{1}{r} P_{22,\theta} + \frac{2}{r} P_{12} = \sin\theta, \tag{6}$$

where P_{ij} are the components of the stress tensor.

From the J_2 flow rule ($P_{ij} - P\delta_{ij} = -\lambda u_{(i;j)}$), $P_{33} = P$, and so the components of the pressure tensor (the negative of the stress tensor) can effectively be restricted to the 1–2 plane, allowing the Drucker-Prager yield condition to be represented by Sokolovski variables (P, γ)

$$P_{11} = P(1 - \sin\phi\cos 2\gamma), \qquad P_{22} = P(1 + \sin\phi\cos 2\gamma), \tag{7, 8}$$

$$P_{12} = -P\sin\phi\sin 2\gamma, \tag{9}$$

where ϕ is the internal angle of friction, and for $\theta \geq 0$, γ is the clockwise angle from the radial to the maximum stress direction. The choice of signs in (7–9) follows because the largest principal pressure is horizontal (because $\gamma(0) = 0$). The ratio of principal pressures equals $(1 + \sin\phi)/(1 - \sin\phi)$.

The flow rule connects the velocity and the Sokolovski angle through

$$\tan 2\gamma = -\frac{T_{,\theta}}{2T} \tag{10}$$

and so

$$T = T_0 e^{-2\int_0^\theta \tan 2\gamma \, d\theta} \tag{11}$$

where T_0 is a constant.

At the walls, where $\theta = \pm\theta_w$, the shear stress $P_{\theta r} = P_{12}$ is assumed equal to the wall coefficient of friction ($\tan\phi_w$) times the normal stress $P_{\theta\theta} = P_{22}$,

$$P_{12} = \mp \tan\phi_w P_{22} \quad \text{at} \quad \theta = \pm\theta_\mathrm{w} \tag{12}$$

and so from (7) and (8)

$$2\gamma_w = \phi_w + \arcsin\left(\frac{\sin\phi_w}{\sin\phi}\right). \tag{13}$$

We shall later require that, at the outlet of the hopper, P is zero at $r=1$ and $\theta=\theta_w$.

The equations above are somewhat unusual, because the two equations in (5) and (6) are partial differential equations involving both r and θ, with the unknown P involvs both r and θ, while γ only involving θ. Consequently, there is the possibility that the equations above may overdetermine the unknowns; showing this is the main aim for the remainder of this section.

Substituting (7–9) in (5) and (6) yields

$$(1-\sin\phi\cos 2\gamma)P_{,r} - \frac{\sin\phi\sin 2\gamma}{r}P_{,\theta} - \frac{2\sin\phi\cos 2\gamma(1+\gamma_{,\theta})}{r}P = \frac{T^2}{r^3} - \cos\theta, \tag{14}$$

$$\sin\phi\sin 2\gamma P_{,r} - \frac{(1+\sin\phi\cos 2\gamma)}{r}P_{,\theta} + \frac{2\sin\phi\sin 2\gamma(1+\gamma_{,\theta})}{r}P = -\sin\theta, \tag{15}$$

multiplying (14) by $\sin 2\gamma$, and adding to $\cos 2\gamma$ times (15) leads to a linear equation in P

$$\sin 2\gamma P_{,r} - \frac{(\cos 2\gamma + \sin\phi)}{r}P_{,\theta} = \frac{T^2\sin 2\gamma}{r^3} - \sin(2\gamma+\theta) \tag{16}$$

which has as its general solution

$$P = f(r\alpha) + ar - \frac{b}{r^2}, \tag{17}$$

where f is an arbitrary function,

$$\alpha = \exp\left(\int_0^\theta \frac{\sin 2\gamma \,\mathrm{d}\theta}{\cos 2\gamma + \sin\phi}\right), \qquad \beta = \exp\left(-\int_0^\theta \frac{2\sin 2\gamma\,\mathrm{d}\theta}{\cos 2\gamma+\sin\phi}\right) = \alpha^{-2}, \tag{18, 19}$$

$$a = \left(\int_0^\theta \frac{\sin(2\gamma+\theta)\mathrm{d}\theta}{(\cos 2\gamma+\sin\phi)\alpha}\right)\alpha, \qquad b = \left(\int_0^\theta \frac{T^2\sin 2\gamma\,\mathrm{d}\theta}{(\cos 2\gamma+\sin\phi)\beta}\right)\beta, \tag{20, 21}$$

where we have set $a(0)=0=b(0)$.

The function f can be found by substituting (17) in (14) and setting θ to zero,

$$(1-\sin\phi)f_{,r} - \frac{2\sin\phi(\gamma_{,\theta}(0)+1)}{r}f = \frac{T^2(0)}{r^3} - 1. \tag{22}$$

The general solution of (22) is

$$f = Kr^\omega + \frac{r}{(\omega-1)(1-\sin\phi)} - \frac{T^2(0)}{(\omega+2)(1-\sin\phi)r^2}, \tag{23}$$

where

$$\omega = \frac{2\sin\phi(1+\gamma_{,\theta}(0))}{1-\sin\phi} \tag{24}$$

and K is a constant. The constant K is found by substituting (23) in (17) and setting P to zero at $r=1, \theta=\theta_w$. This fixes P, given γ and the constant $T(0)$. Consequently the functional form of P is the sum of terms of the form r^{ω}, r, r^{-2}, and so when this result is substituted in (14), three equations are obtained for $\gamma_{,\theta}$, making this system overdetermined. Hence, no solutions to the freely discharging hoppper problem exist with only one radial velocity component.

3. Recap

The conclusion that no wholly radial velocity solution exists for a freely discharging hopper is a surprising and disappointing result. Four alternatives suggest themselves. Firstly, no steady-flow solutions may exist to the plastic flow equations. (Here I am disregarding the radial solution of Jenike [10], which is only valid for zero velocity, and so cannot describe exactly a freely discharging hopper.) The non-existence of steady plastic flows from a freely discharging hopper is a possibility, but has not been proven. However, the exact (non-radial) solution of Weir [12] provides some hope that exact steady solutions may exist.

The second alternative is that steady, though discontinuous velocity solutions exist. Such discontinuous flows have been observed recently in numerical analyses by Gremaud *et al.* [13] for non-inertial flows. Discontinuous flows are perhaps implied in the work of Kaza and Jackson [14], and are compatible with the hyperbolic nature of the plastic-flow equations.

The third alternative is that steady radial solutions may exist, but the flow rule assumed above is incorrect, and should be disregarded. When this is done, exact solutions can be obtained for $P = a_1(\theta)r - b_1(\theta)r^{-2}$, by imposing (4) and (7–9), since then four equations result from (7) and (8), one of which fixes the angular distribution of u_1. Calculations (not shown here) reveal that, for steep hoppers, the typical radial velocity increases with θ, whereas intuition and experiment suggest the opposite. Hence, the alternative of disregarding the flow rule must be dismissed.

The fourth alternative is that steady continuous solutions exist, but the flow necessarily has two components. Within this fourth alternative, two separate limiting possibilities suggest themselves. Firstly, as the radius increases without limit, the solution could tend to the radial solution of Jenike [10]. This is implied in essentially all previous analyses of hopper flow. In this possibility, a plastic flow solution would exist over an infinite domain. In the second possibility, as the radius tends to infinity, the flow could tend to an inner non-plastic vertical funnel flow and an outer stagnant region, and the region of plastic flow is finite about the orifice. Which of these two possibilities arises depends on the rate at which the perturbation to radial flow increases with distance, relative to the radial flow approximation.

Numerical solutions [15] of the non-inertial plastic-flow equations suggest that for large radii the flow does indeed tend towards the (zero velocity) radial solution, supporting the idea of an infinite region of plasticity. However, experimental work by Baxter *et al.* [3] suggests that hopper flows tend from mass to funnel flow as the radius increases, supporting the idea of a finite region of plasticity. In the next section we assume plasticity occurs everywhere.

4. Non-radial flow

Incompressible flow in a wedge-shaped hopper implies the existence of a function χ, with

$$u_1 = \frac{1}{r}\chi_{,\theta}, \qquad u_2 = -\chi_{,r}, \tag{25, 26}$$

where u_1, u_2 are the radial and axial components of velocity.

The J_2 flow rule and the Drucker-Prager yield condition imply that the components of stress still satisfy (7–9), but now γ is a function of both r and θ.

The non-dimensional Newton-force equations are

$$u_1 u_{1,r} + \frac{u_2}{r}u_{1,\theta} - \frac{u_2^2}{r} + P_{11,r} + \frac{1}{r}P_{12,\theta} + \frac{(P_{11} - P_{22})}{r} = -\cos\theta, \tag{27}$$

$$u_1 u_{2,r} + \frac{u_2}{r}u_{2,\theta} + \frac{u_1 u_2}{r} + P_{12,r} + \frac{1}{r}P_{22,\theta} + \frac{2}{r}P_{12} = \sin\theta. \tag{28}$$

From the ratio of $P_{12}/(P_{22} - P)$ a relationship is found connecting γ and χ,

$$\tan 2\gamma = \frac{1/r^2 \chi_{,\theta,\theta} - \chi_{,r,r} + \frac{1}{r}\chi_{,r}}{2\left(\frac{\chi_{,\theta}}{r}\right)_{,r}}. \tag{29}$$

Since γ equals γ_w in (13) for $r \geq 1$ and $\theta = \theta_w$, (13) and (29) impose one condition on χ at the walls. Another condition is that u_2 and $\chi_{,r}$ are both zero (χ constant) at the walls, which are assumed to be containing. A third condition on χ for symmetric flows is that $\chi = 0$ along the axis $\theta = 0$. Equation (29) can be used to replace γ in the equations above, and this results in two third-order equations from (27) and (28) for χ. The remaining variable P is contained in two first-order relationships in (27) and (28).

In this section we shall follow the work of Kaza and Jackson [11], and seek a series solution of the equations above using

$$\chi = \Sigma_{n=0}^{\infty}\chi_n(\theta)r^{-3n}, \qquad P = \Sigma_{n=0}^{\infty}P_n(\theta)r^{1-3n}, \qquad \gamma = \Sigma_{n=0}^{\infty}\gamma_n(\theta)r^{-3n}. \tag{30, 31, 32}$$

We seek a solution with χ and P even in θ and γ odd in θ, and satisfying the boundary conditions

$$\chi_n(0) = 0, \qquad \chi_n(\theta_w) = \chi_0(\theta_w)\delta_{n,0}, \tag{33, 34}$$

$$\Sigma_{n=0}^{\infty}P_n(\theta_w) = 0, \qquad \gamma_n(0) = 0, \qquad \gamma_n(\theta_w) = \gamma_w\delta_{n,0}, \tag{35, 36, 37}$$

where $\delta_{n,0}$ is the Kronecker delta function (equalling unity when n is zero, zero otherwise).

The only inertial terms contributing to zero and first order arise from the $u_1 u_{1,r}$ term. The zero; and first-order equations from (27), (28) and (30–32) are

$$(P_0 \sin\phi \sin 2\gamma_0)_{,\theta} = \cos\theta + (1 - 3\sin\phi\cos 2\gamma_0)P_0, \tag{38}$$

$$(P_0(1 + \sin\phi\cos 2\gamma_0))_{,\theta} = \sin\theta + 3P_0\sin\phi\sin 2\gamma_0, \tag{39}$$

$$\sin\phi(2P_0\cos 2\gamma_0\gamma_1 + P_1\sin 2\gamma_0)_{,\theta} = -(\chi_{0,\theta})^2 - 2P_1, \tag{40}$$

$$((1 + \sin\phi\cos 2\gamma_0)P_1)_{,\theta} = (2P_0\sin\phi\sin 2\gamma_0\gamma_1)_{,\theta}, \tag{41}$$

where to second order

$$\cos 2\gamma = \cos 2\gamma_0 - \frac{2\sin 2\gamma_0\gamma_1}{r^3}, \qquad \sin 2\gamma = \sin 2\gamma_0 + \frac{2\cos 2\gamma_0\gamma_1}{r^3}. \tag{42, 43}$$

From (29) the zero- and first-order terms give

$$\chi_{0,\theta,\theta} = -2\tan 2\gamma_0 \chi_{0,\theta}, \qquad \chi_{1,\theta,\theta} + 8\tan 2\gamma_0 \chi_{1,\theta} - 15\chi_1 = -\frac{4\gamma_1 \chi_{0,\theta}}{\cos^2 2\gamma_0} \tag{44, 45}$$

and so

$$\chi_{0,\theta} = -T_0 \exp\left(-2\int_0^\theta \tan 2\gamma_0 \mathrm{d}\theta\right) = -T_0 F, \tag{46}$$

where $T_0 = -\chi_{0,\theta}(0)$ is a positive constant. The boundary conditions in (33) and (34) and (44–45) fix χ_0 and χ_1, and so (25) and (26) fixes the zero- and first-order velocity components.

The equations above can be rewritten in essentially standard form for numerical solution as

$$(\cos 2\gamma_0 + \sin\phi) P_{0,\theta} = \sin(2\gamma_0 + \theta) + \sin 2\gamma_0 P_0, \tag{47}$$

$$\begin{aligned} 2\sin\phi(\cos 2\gamma_0 + \sin\phi) P_0 \gamma_{0,\theta} = {} & \cos\theta + \sin\phi\cos(2\gamma_0+\theta) \\ & + P_0(1 - 2\sin\phi\cos 2\gamma_0 - 3\sin^2\phi), \end{aligned} \tag{48}$$

$$(\cos 2\gamma_0 + \sin\phi) P_{1,\theta} = 4\gamma_1 \sin\phi P_0 \gamma_{0,\theta} - \sin 2\gamma_0 F^2 T_0^2 - 2P_1 \sin 2\gamma_0, \tag{49}$$

$$\begin{aligned} 2\sin\phi(\cos 2\gamma_0 + \sin\phi) P_0 \gamma_{1,\theta} = {} & \sin^2\phi \sin 2\gamma_0 (P_1(\cos 2\gamma_0)_{,\theta} - 2\gamma_1(P_0 \sin 2\gamma_0)_{,\theta}) \\ & - (1 + \sin\phi\cos 2\gamma_0)(F^2 T_0^2 + 2P_1) \\ & + \sin\phi\gamma_1(2P_0\cos 2\gamma_0)_{,\theta} + \sin\phi P_1(\sin 2\gamma_0)_{,\theta}, \end{aligned} \tag{50}$$

$$F_{,\theta} = -2\tan 2\gamma_0 F. \tag{51}$$

We shall truncate the series expansions in (30–32) after two terms, which implies the following conditions from (33–37)

$$P_0(0) = \frac{1}{3\sin\phi + 2\sin\phi\gamma_{0,\theta}(0) - 1}, \qquad P_1(0) = \frac{(1+\sin\phi\cos 2\gamma_w)P_0(\theta_w)}{1+\sin\phi}, \tag{52, 53}$$

$$P_1(\theta_w) = \frac{(1+\sin\phi)P_1(0)}{1+\sin\phi\cos 2\theta_w}, \qquad F(0) = 1, \tag{54, 55}$$

which are useful for initial estimates of the P_0, P_1.

Equations (47–51) are five ordinary equations for the five unknown functions $P_0, \gamma_0, P_1, \gamma_1, F$. There are six boundary conditions above in (33–37) and (55), which allow these equations to be solved, and the constant T_0 to be found. These equations are essentially those in Kaza and Jackson [11], except that here the total flow is unknown, and must be derived from the known geometry. In Kaza and Jackson's work, the flow is given, and the geometry is adjusted to agree with the given total flow.

5. Numerical results

In this section we shall set $\phi_w = 0{\cdot}5\phi$, which is approximately true for aluminium walls. All of the parameters above are then functions of the two variables ϕ, θ_w.

Figure 1 plots the variation of P_0 as a function of θ and ϕ. The equation for P_0 is that for pressure in Jenike's radial solution, except that here the boundary condition on P_0 depends on

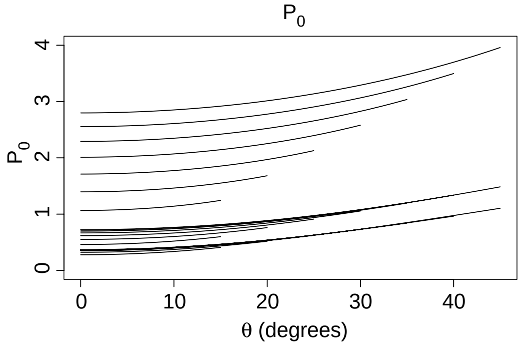

Figure 1. Variation of P_0 as a function of θ for θ_w = 15°, 20°, 25°, 30°, 35°, 40° and 45°; and for ϕ = 20°, 30° and 40°. Each of the 21 curves terminate at its θ_w value. For a given value of θ_w, the three curves for the different values of ϕ are ordered up the page, starting from ϕ = 20° at the bottom, to ϕ = 40° at the top of the figure.

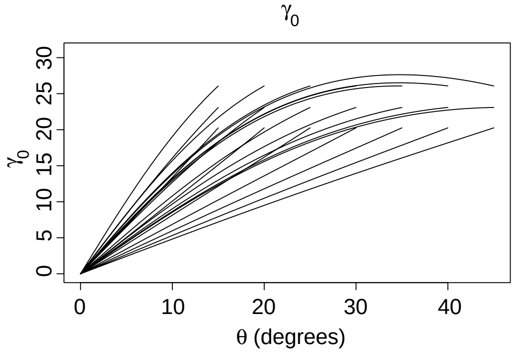

Figure 2. Variation of γ_1 as a function of θ. As for Figure 1.

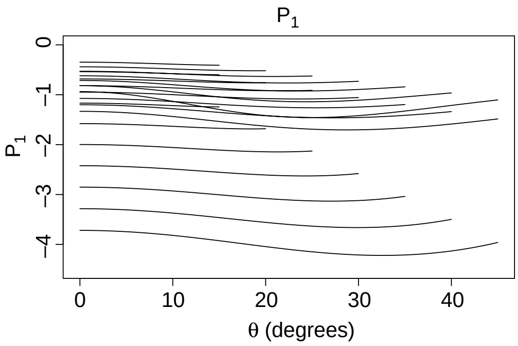

Figure 3. Variation of P_1 as a function of θ. As for Figure 1, but with ϕ values increasing down the page.

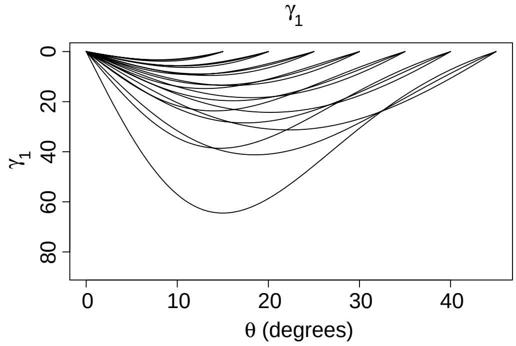

Figure 4. Variation of γ_1 as a function of θ. As for Figure 1, but with ϕ values decreasing down the page to the left of the Figure.

that for P_1 (via (35)). Similarly, the angular dependence of γ_0 is given in degrees in Figure 2, and again is just that of the Sokolovski coordinate in Jenike's radial solution.

The corresponding plot for P_1 is given in Figure 3. In contrast to P_0, P_1 is always negative, in order that P is zero at the orifice edge. Similarly, γ_1 is given in Figure 4, and is also always negative, but as θ increases, the curves for γ_1 show a change of sign in their curvature. The corresponding curves for F are given in Figure 5 for completeness, as these are just the corresponding curves for Jenike's radial solution.

A plot of the total pressure $P_0 r + P_1/r^2$ is given in Figure 6 for $\phi = 30°$ and $\theta_w = 30°$. The concave-downwards contours are typical of the pressure contours when θ_w is not too large for a given ϕ. Only positive pressures are valid, so the region below the zero contour needs to be omitted from consideration.

An extreme example of the variation of P with position is shown in Figure 7, for very high values of friction angle. An internal maximum of P clearly occurs about the orifice along the P = 0 contour, which suggests that a transition to funnel flow should occur in this example, as the pressure field separates the flow internally.

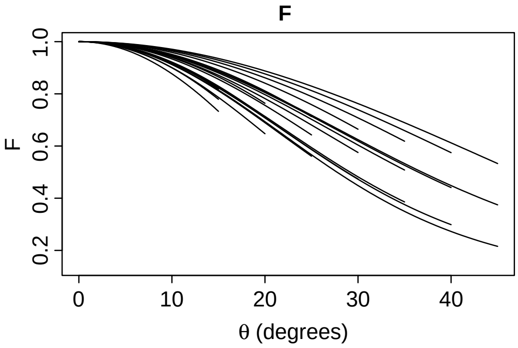

Figure 5. Variation of F as a function of θ. As for Figure 1, but with ϕ increasing down the page.

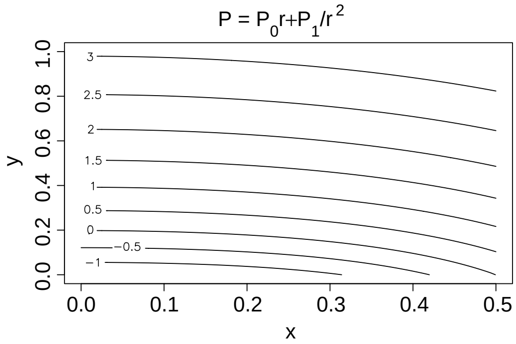

Figure 6. Contour plot of $P_0r + P_1r^{-2}$ about the orifice. Lengths are scaled so that the orifice width is 2 $\sin\theta_w$. Ordinate is scaled height above the orifice opening. θ_w = 30° and ϕ = 20°.

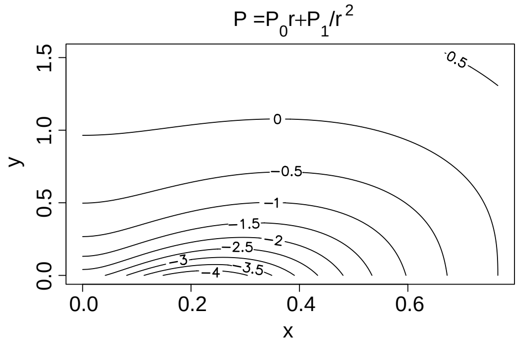

Figure 7. Contour plot of $P_0r + P_1r^{-2}$ about the orifice. Lengths are scaled so that the orifice width is 2 $\sin\theta_w$. Ordinate is scaled height above the orifice opening. θ_w = 50° and ϕ = 45°.

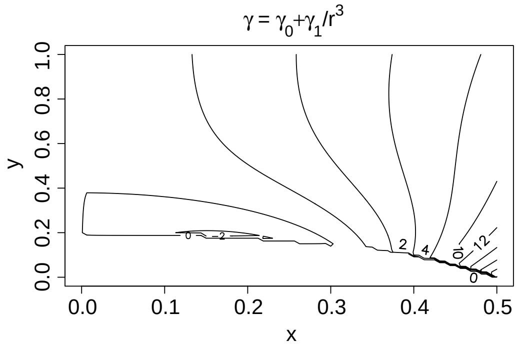

Figure 8. Contour plot of $\gamma_0+\gamma_1 r^{-3}$ about the orifice, for $\theta_w=30°$, and $\phi=20°$. Lengths are scaled so that the orifice width is 2 sin θ_w. Ordinate is scaled height above the orifice opening. Contours are truncated at the $P=0$ contour.

A plot of γ to second order, $\gamma_0+\gamma_1 r^{-3}$, is given in Figure 8 about the orifice for $\phi=20°$ and $\theta_w=30°$. Far above the orifice, γ tends quickly to the radial function γ_0, but near the middle of the orifice, γ becomes negative, and these negative values extend above the zero pressure contour (where the γ contours are truncated). The surface γ = 0 corresponds to a surface of zero shear stress, from (9).

As θ_w is increased much beyond ϕ, where mass flow will have ceased, the negative values of γ above the zero pressure contour become more extreme, and can drop below −45°, which means the analysis above has failed, since then (29) is undefined.This failure can be associated with the failure of mass flow, because a very large γ in (11) implies a very small velocity in (4), *i.e.*, a tendency towards funnel flow. For such extreme and invalid examples, the zero-pressure contour has a maximum away from the centre of the orifice. An example of such extreme behaviour is shown in Figure 9, which shows the zero pressure contour and the invalid values of γ. Clearly, the results in this paper require the values of θ_w to be not too large, for a given value of ϕ. This is also implied in the expansion in (42) and (43).

Parameter values for which mass flow is expected, have axial velocity components u_2 which are much smaller than the corresponding radial velocity component u_1. Examples of these

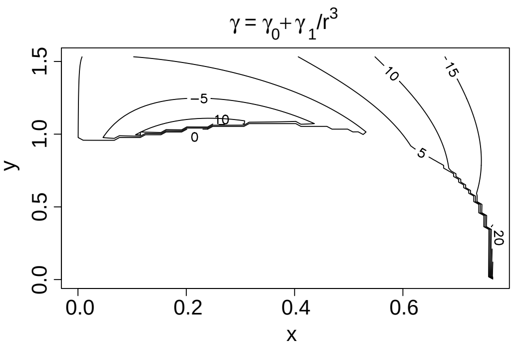

Figure 9. Contour plot of $\gamma_0+\gamma_1 r^{-3}$ about the orifice, for $\theta_w=50°$ and $\phi=45°$. Lengths are scaled so that the orifice width is 2 sin θ_w. Ordinate is scaled height above the orifice opening. Contours are truncated at the $P=0$ contour.

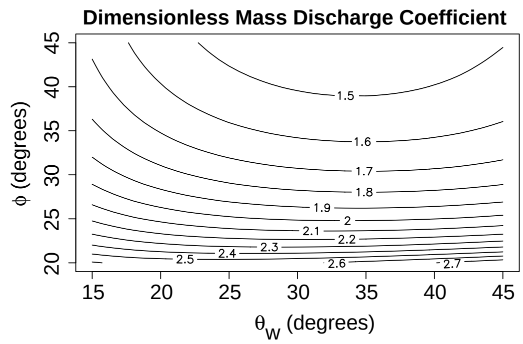

Figure 10. Contour plot of the discharge coefficient C in (57) as a function of θ_w and ϕ.

are not shown here, but the radial velocity component is always negative, and the axial component is always positive, which will tend to slightly divert the velocity flow direction from radial towards the vertical. This was also found by Kaza and Jackson [11].

From (2), (3), (25), (33–34) and (46), the mass discharge from the hopper can be written as

$$\dot{M}=C\rho L W^{\frac{3}{2}}\sqrt{g}, \tag{56}$$

where L is the length of the hopper, W its width, and C the non-dimensional mass-discharge coefficient

$$C=-\frac{\chi_0(\theta_w)}{\sqrt{2}\sin^{\frac{3}{2}}(\theta_w)}=\frac{T_0}{\sqrt{2}\sin^{\frac{3}{2}}(\theta_w)}\int_0^{\theta_w}F\,\mathrm{d}\theta \tag{57}$$

Figure 10 plots contours of C as a function of θ_w and ϕ. In contrast to experimental data, which strongly suggests that the mass discharge is a monotonically decreasing function of θ_w, Figure 10 shows a minimum mass discharge as θ_w varies, for fixed ϕ. This is suggestive of the mass-funnel flow transition, because for θ_w sufficiently large, it is easier for the flow to be confined within a more steeply angled boundary, as occurs in funnel flow.

If only small values of θ are considered, well before the minimum in the contour of C is reached, then C can be written as

$$C=\frac{h(\phi)}{(\tan(\theta_w))^m} \tag{58}$$

for some exponent m, and some function h. For example, from Figure 10, the exponent m for $\phi=25°, 30°, 40°$ is about 0·17, 0·27 and 0·32, respectively, for θ_w about 15°. Clearly, for these small values of θ_w, the exponent m increases with ϕ. This is opposite to the report in the reference of Laird and Roberts [16] that the exponent m is greater for ballotini than for sand, although ϕ for ballotini should be smaller than for sand. To agree with the empirical discharge law of Nedderman *et al.* [5] requires $C=1{\cdot}03(\tan\Theta/\tan\theta_w)^{0{\cdot}2}$ where Θ is the (unspecified) angle for the mass-funnel transition.

Finally, contours of the value of r where P is zero on the axis $\theta=0$ is plotted in Figure 11.

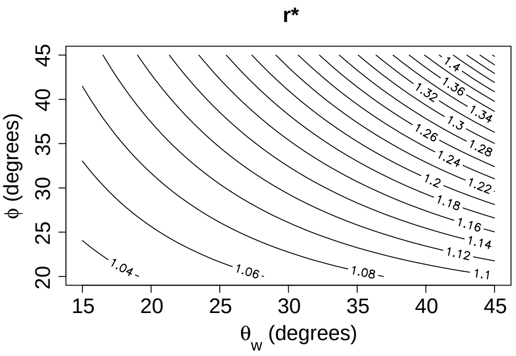

Figure 11. Contour plot of the r value where $P(r, 0)$ is zero, as functions of ϕ and θ_w.

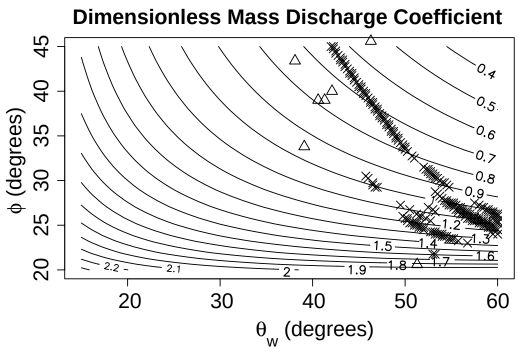

Figure 12. Contour plot of the discharge coefficient C in (57) and (60) as a function of θ_w and ϕ.

6. Axial approximation

Section 4 coupled the radial solution of Jenike with higher-order terms, using the series expansion of Kaza and Jackson [11], thereby allowing the zero-pressure condition to be imposed at the edge of the orifice. However, this analysis was asymptotic, valid for large values of r, and may be poor about the orifice (as found by Kaza and Jackson). Specifically, at the orifice, the momentum terms coupled only weakly to gravity. We would expect the zero-order terms in velocity to couple directly to gravity at the orifice, because these terms are determining the discharge, whereas only the zero-order terms in pressure coupled directly to gravity.

However, when an expansion is sought in which velocity couples directly to gravity, we find the leading terms are $\chi = \chi_0 r^{1\cdot 5}$, $P = P_0 r$, $\gamma = \gamma_0$, which are unacceptable because this predicts unbounded velocities for large r. To overcome this problem, the angular variation of variables is chosen from those in Section 4, but the radial variation of pressure is found by setting $\theta = 0$ in (27), giving the axial pressure equation

$$(1 - \sin\phi) P_{,r} - \frac{2P(1 + \gamma_{0,\theta})(0)\sin\phi}{r} = -1 + \frac{T_0^2}{r^3}, \tag{59}$$

where, from (25) and (30) to first order, along the axis $u_1 = -T_0/r$, and T_0 is a constant. The solution of (59) is of the form $P = Ar - Br^{-2}$ for unlimited hoppers, and so requiring $P = 0$ at $r = r_0$ yields

$$T_0^2 = \frac{2(1 + \gamma_{0,\theta}(0)\sin\phi) r_0^3}{3\sin\phi + 2\gamma_{0,\theta}(0)\sin\phi - 1}, \tag{60}$$

where r_0 is the value of r (close to unity) where $P = 0$ on the axis for the functions in Section 4. The dependence of r_0 is given in Figure 11.

This value of T_0 is now used in (57) and the corresponding contours are plotted in Figure 12. Also plotted in Figure 12 as triangles are measurements of the parameter values corresponding to some failure surfaces in wedge-shaped hoppers [17], indicating the transition between mass and funnel flow.

Also plotted in Figure 12 as crosses are the points where the numerical code failed to find solutions to the equations in Section 4 to a high degree of accuracy. The location of these crosses depends on the tolerances requested. Figure 12 has been constructed with only

Table 1. Nomenclature.

a	function of θ, (20)	R	dimensional radial coordinate, (2)
A	constant	R_1	dimensional radial coordinate of orifice boundary, (1)
b	function of θ, (21)	T	angular behaviour of u_1, (4)
B	constant	T_0	T on the axis $\theta=0$, (11)
C	non-dimensional mass flow coefficient	u_1	non-dimensionless radial velocity component, (4)
E	constant, (A2)	u_2	non-dimensionless axial velocity component, (26)
f	function of θ, (22)	U_1	dimensional radial velocity component, (3)
F	function of θ	W	width of wedge
g	gravitational accelertion	Z	function of θ, (A7)
G	function of θ, (A6)	α	function of θ, (18)
h	function of ϕ, (58)	β	function of θ, (19)
K	constant	χ	potential flow function, (25)
L	length of wedge	χ_n	function of θ, (33)
$\dot{M}$	mass discharge rate	γ	Sokolovski angle, (7)
m	exponent	γ_n	function of θ
M	function of θ, (A5)	γ_w	Sokolovski angle at wall, (13)
n	summation index, (33)	$\delta_{n,0}$	Kronecker delta function
p	dimensional pressure	θ	angular variable
P	dimensionless pressure	θ_w	half hopper angle
P_n	dimensionless pressure component, function of θ	ρ	solid bulk density
P_{ij}	dimensionless pressure tensor, (5)	ω	constant, (24)
Q	function of θ, (A4)	ϕ	internal angle of friction, (7)
r	non-dimensional radial coordinate, (2)	ϕ_w	angle of wall friction
r_0	non-dimensional radius where $P(r_0, 0)=0$		
r_1	non-dimensional radial coordinate of orifice boundary		

3-significant-figure accuracy, in order to obtain a sharp boundary for the region separating convergence and non-convergence of the numerical code. It is seen that this numerical boundary of parametric sensitivity tends to be slightly greater than the boundary for the mass-funnel flow transition, which is difficult to specify accurately, because of what appears to be significant scatter in the experimental record.

7. Conclusions

This paper contains three new results. Firstly, it was shown in Section 2 that radial-flow solutions do not exist for plastic flows satisfying a Drucker-Prager yield law and the J_2 flow-rule, in a wedge-shaped hopper. This new result is interesting because of the significance of radial flows in previous analytical work.

The mathematical framework developed by Kaza and Jackson [11] was used to obtain approximations for velocity and stresses in a wedge-shaped hopper operating in mass flow. Extensive results were obtained by allowing the internal friction angle and wedge opening angle to vary significantly. Plots were obtained of the zero-pressure contour about the orifice, and the effect of the non-radial flows is to divert the radial flow to being more vertical near the orifice.

Secondly, an improved estimate for mass discharge was obtained in Section 6 by solving the pressure equation along the axis $\theta=0$, and using the angular variation of variables found in Section 4. The dimensionless mass-discharge coefficient was plotted in Figure 12, and showed that mass discharge decreases monotonically with internal friction angle ϕ, and (usually) with opening angle θ_w.

The predicted dependence of mass discharge on θ_w and ϕ was more complicated than shown in previous correlations with θ_w. Specifically, the exponent of $\tan\theta_w$ is predicted to vary with ϕ. Exact comparison with experiment was not attempted here, because these previous correlations scale discharge with failure angle, but do not provide a rule for calculating the failure angle. For convenience, all calculations in this paper assumed that the angle of wall friction was one half of the internal friction angle. However, all of the plots in this paper can in principle be varied by allowing the ratio between ϕ_w to ϕ to vary.

Thirdly, the new equations for P_1, γ_1, χ_1 in (49), (50) and (45) respectively, can not always be solved numerically to arbitrary precision as ϕ and θ_w increase. A definite line of singular values exist, shown in Figure 12 as crosses, where the equations did not allow a numerical solution to the requested tolerance. The failure of these equations to yield a numerical solution is closely related to the development of an internal maximum in the pressure field about the orifice. These two effects suggest a conservative estimate for the mass-funnel transition in hopper flows, although both boundaries are subject to significant scatter. Note that the first-order equations do have exact analytical solutions, as shown in Appendix A, suggesting the mass-funnel transition may result from an instability, rather than from a singularity, because the coefficient of T_0^2 in (A8) is always non-zero.

Appendix. Analytical solution of first order terms

From (41),

$$(1+\sin\phi\cos 2\gamma_0)P_1 = (2P_0\sin\phi\sin 2\gamma_0\gamma_1) - E, \tag{A1}$$

where E is a constant of integration.

From (35, 36, 37), $P_0(\theta_w)+P_1(\theta_w) = 0$, and so from (61),

$$E = (1+\sin\phi\cos 2\gamma_w)P_0(\theta_w) \tag{A2}$$

which fixes P_1.

Substituting (A1) in (40) gives a linear equation for γ_1, which can be written in the form

$$Z = (MQ)_{,\theta}, \qquad Q = \frac{2\sin\phi P_0\gamma_1}{(1+\sin\phi\cos 2\gamma_0)}, \qquad M = (\sin\phi+\cos 2\gamma_0)G, \qquad \text{(A3, A4, A5)}$$

$$G = \exp\left(\int_0^\theta \frac{2\sin 2\gamma_0 \mathrm{d}\theta}{(\sin\phi+\cos 2\gamma_0)}\right), \tag{A6}$$

$$Z = G\left[\frac{2E}{1+\sin\phi\cos 2\gamma_0} + \left(\frac{\sin\phi E\sin 2\gamma_0}{(1+\sin\phi\cos 2\gamma_0)}\right)_{,\theta} - T_0^2F^2\right] \tag{A7}$$

and so from (36) and (37),

$$\int_0^{\theta_w} Z\mathrm{d}\theta = 0, \tag{A8}$$

because Q in (A4) is proportional to γ_1, and so (A8) fixes the the zero-order mean discharge speed T_0, because of the linear appearance of T_0^2 in (A7).

Acknowledgements

The figures have been calculated by Peter McGavin. The author is indebted to referee Dr Scott McCue for pointing out the paper by Kaza and Jackson.

References

1. D.G. Schaeffer, Instability in the evolution equations describing incompresible granular flow. *J. Diff. Equ.* 66 (1987) 19–50.
2. K.C. Valanis and J.F. Peters, Ill-posedness of the initial and boundary value problems in non-associative plasticity. *Acta Mech.* 114 (1996) 1–25.
3. G.W. Baxter, R.P. Behringer, T. Fagert and G.A. Johnson, Pattern formation and time-dependence in flowing sand. In: D.D. Joseph and D.G. Schaeffer (eds.), *Two-Phase Flows and Waves*. Berlin: Springer-Verlag (1990) pp.1–28.
4. H.B. Mulhaus and I. Vardoulaki, The thickness of shear bands in granular materials. *Geotechnique* 37 (1987) 271–283.
5. R.M. Nedderman, U. Tuzun, S.B. Savage and G.T. Houlsby, Review Article Number 10: The flow of granular materials: Discharge rates from hopper. *Chem. Eng. Sci.* 37 (1982) 1597–1609.
6. R.L. Brown and J.C. Richards, Profile of flow of granules through apertures. *Trans. Inst. Chem. Engng.* 38 (1960) 243–250.
7. W.A. Beverloo, H.A. Leniger and J. van de Velde, The flow of granular solids through orifices. *Chem. Eng. Sci.* 15 (1961) 260–269.
8. C. Brennen and J.C. Pearce, Granular material flow in two-dimensional hoppers. *J. Appl. Mech.* 45 (1978) 43–50.
9. T.V. Nguyen, C. Brennen and R.H. Sabersky, Gravity flow of granular materials in conical hoppers. *J. Appl. Mech.* 46 (1979) 529–535.
10. A.W. Jenike, Steady gravity flow of frictional-cohesive solids in converging channels. *J. Appl. Mech.* 31 (1964) 5–11.
11. K.R. Kaza and R. Jackson, The rate of discharge of coarse granular material from a wedge-shaped mass flow hopper. *Powder Technol*. 33 (1982) 223–237.
12. G.J. Weir, The intrinsic cohesion of granular materials. *Powder Technol*. 104 (1999) 29–36.
13. P.A. Gremaud, J.V. Matthews and M. Shearer, Similarity solutions for hopper flows. In: J. Bona, K. Saxton and R. Saxton (eds.), *Nonlinear PDEs, Dynamics and Continuum Physics*. Providence, Rhode Island: AMS Contempory Mathematics, Series 255 (2000) pp. 79–95.
14. K.R. Kaza and R. Jackson, Boundary conditions for a granular material flowing out of a hopper or bin. *Chem. Eng. Sci.* 39 (1984) 915–916.
15. J.J. Johanson and A.W. Jenike, *Stress and Velocity Fields in Gravity Flow of Bulk Solids.* Salt Lake City, Utah: Bulletin No. 116, Bulletin of the University of Utah 53 (21) (1962) 138 pp.
16. B.W. Laird and P.M. Roberts, *Chemical Engineering*. Tripos, Part 2. Research Project Report, University of Cambridge (1979).
17. R.L. Brown and J.C. Richards, Kinematics of the flow of dry powders and bulk solids. *Rheology Acta* 4 (1965) 153–165.